# Single-chain simulation of Ising density functional theory for weak polyelectrolytes

Alejandro Gallegos[1], Marcus Müller[2], and Jianzhong Wu[1*]

[1]*Department of Chemical and Environmental Engineering, University of California, Riverside, CA 92521, USA*

[2]*Institut für Theoretische Physik, Georg-August- Universität, 37077, Göttingen, Germany*

## Abstract

The conventional theories of weak polyelectrolytes are either computationally prohibitive to account for the multidimensional inhomogeneity of polymer ionization in a liquid environment or oversimplistic in describing the coupling effects of ion-explicit electrostatic interactions and long-range intrachain correlations. To bridge this gap, we implement the Ising density functional theory (iDFT) for ionizable polymer systems using the single-chain-in-mean-field (SCMF) algorithm. The single-chain-in-Ising-density-functional-theory (sc-iDFT) shows significant improvements over conventional mean-field methods in describing segment-level dissociation equilibrium, specific ion effects, and long-range intrachain correlations. With an explicit consideration of the fluctuations of polymer configurations and the position-dependent ionization of individual polymer segments, sc-iDFT provides a faithful description of the structure and thermodynamic properties of inhomogeneous weak polyelectrolyte systems across multiple length scales.

**Keywords**:

Single-chain-in-mean-field simulation, polymer density functional theory, charge regulation

[*]To whom correspondence should be addressed. Email: jwu@engr.ucr.edu

## 1. Introduction

Weak polyelectrolytes play a critical role in a wide variety of biological processes and are broadly utilized in technological applications such as water treatment, bioadhesive materials, and gene delivery[1-4]. The diverse functionality of weak polyelectrolytes is largely attributed to the adaptability of the electrostatic charge and polymer configurations to external stimuli and local solution conditions. Numerous studies have been devoted to understanding the adaptable behavior of weak polyelectrolyte systems[5-8]. However, it remains theoretically challenging to predict both structure and thermodynamic properties from a molecular perspective due to the complex interplay of monomeric ionization with polymer configurations. Existing theoretical methods, including the Poisson-Boltzmann (PB) equation[9, 10], polymer scaling analysis[11, 12], self-consistent-field theory[13-15], and coarse-grained molecular models[16-18], typically describe the coupling effects between the average charge and the configuration of weak polyelectrolyte chains without an explicit consideration of the ionization of individual segments and salt ions. Meanwhile, molecular simulation methods are mostly applied to relatively short polymer chains or often limited by a narrow range of solution pH.[19-22] While mean-field theories have been quite successful in capturing certain aspects of weak polyelectrolyte systems, they are in general not able to account for explicit-ion effects and long-range intrachain correlations and therefore have limited capability in predicting the functionality of realistic weak polyelectrolyte systems.

Recently, we developed a new theoretical framework for inhomogeneous weak polyelectrolyte systems by combining the Ising-chain model for ionization with the polymer density functional theory[23]. In principle, the so-called Ising density functional theory (iDFT) provides an exact theoretical procedure for describing ionizable systems by treating the charge state and the position of each ionizable group on an equal footing. An accurate free-energy

functional can be formulated to account for solvent-mediated interactions, ion-explicit excluded-volume effects, electrostatic interactions, and long-range intrachain correlations. While the theoretical procedure is applicable to both atomic and coarse-grained models of ionizable systems, the numerical difficulty in solving the density profiles of polymer segments limits its application mostly to systems with only one-dimensional inhomogeneity. In this work, we demonstrate that this caveat can be alleviated by implementing iDFT within the framework of the Single-Chain-in-Mean-Field (SCMF) algorithm that temporarily approximates explicit nonbonded interactions between ions, solvent, and polymer chains in terms of effective one-body potentials (*viz*., effective external fields)[24]. Independent polymer chains are simulated in these external fields in order to capture the polymer configurational distributions (i.e., through Monte Carlo sampling of single-chain configurations). The simulation results, in turn, are used to compute the one-body potentials for individual species by utilizing the polymer density functional theory. It should be noted that the quasi-instantaneous field approximation[25] invoked by the SCMF algorithm captures both intermolecular interactions and intrachain correlations explicitly (on long wavelengths) if the polymer configurations vary slowly on the time scale applied to updating the effective external fields and the discretization of space and molecular contour are appropriately chosen. The iterative procedure eschews the direct simulation of the interacting multichain system and allows for an efficient implementation on parallel or GPU-accelerated computers. SCMF also accounts for the interplay between single-chain dynamics and collective kinetics[26]. A previous implementation of the SCMF algorithm for weak polyelectrolyte systems did not consider explicitly the ionization state of individual segments or intrachain electrostatic correlations[24]. In combination with iDFT, the SCMF algorithm will be able to capture both short- and long-range correlations at the segment level. We refer to the new approach as the single-chain-in-Ising-density-functional-theory (sc-

iDFT) because we use the single-chain simulation to sample the polymer configurations in the effective external field determined by iDFT calculations. In this work, we will demonstrate that sc-iDFT improves upon the conventional mean-field methods by accounting for the segment-level ionization behavior of weak polyelectrolytes including the configurations of individual chains with different sequences of ionizable segments.

## 2. Thermodynamic model and methods

### *2.1 Theoretical description of weak polyelectrolyte systems*

We consider an augmented primitive model (APM) for weak polyelectrolyte systems where each polymeric species is represented by tangent hard-sphere chains of ionizable segments, monomeric ionic species by charged hard spheres each with fixed diameter $\sigma_i$ and valence $Z_i$, and the solvent by a dielectric continuum. The reduced pair potential between charged hard spheres separated by distance *r* is given by

$$\beta u_{i,j}\left(r;Z_i,Z_j\right)=\begin{cases}\infty, & r<\sigma_{i,j}\\ \dfrac{l_B}{r}Z_iZ_j & r\geq\sigma_{i,j}\end{cases} \tag{1}$$

where $l_B=e^2/4\pi\varepsilon_0\varepsilon_r k_BT$ denotes the Bjerrum length (7.14 Å for liquid water at room temperature). Other variables in Eq.(1) have their usual meanings, i.e., $e$ represents the elementary charge, $\varepsilon_0$ and $\varepsilon_r$ are the vacuum permittivity and the dielectric constant of the solvent, respectively; $\beta=1/k_BT$, $k_B$ is the Boltzmann constant, $T$ is the absolute temperature, and $\sigma_{i,j}=(\sigma_i+\sigma_j)/2$.

The coarse-grained model accounts for protons and hydroxyl ions explicitly as charged hard spheres. The bulk concentrations of these ions are determined by the solution pH, i.e.,

$c^b_{H^+} = 10^{-\mathrm{pH}} \exp(-\beta\mu^{ex}_{H^+})$, $c^b_{OH^-} = 10^{\mathrm{pH-14}} \exp(-\beta\mu^{ex}_{OH^-})$, and $\mu^{ex}_i$ is the excess chemical potential in the bulk solution. The appropriate expressions for the excess chemical potentials, $\mu^{ex}_i$, as well as the self-consistent determination of the concentrations of all species in the bulk solution (viz. salt ions, protons, and hydroxyl ions) and their molecular parameters can be found in a previous publication[27]. Throughout this work, the solvent is considered as a background with a uniform dielectric constant of $\varepsilon_r = 78.4$.

For a polymer chain with *M* neutral segments, its configuration is fully specified by a multidimensional vector, $\mathbf{R} = (\mathbf{r}_1, \mathbf{r}_2, ..., \mathbf{r}_M)$, where $\mathbf{r}_i$ denotes the position of segment $i$. For a weak polyelectrolyte chain, an additional variable is needed to specify the charge state of the ionizable groups. With the assumption that all polymer segments are ionizable, the latter can be specified by an *M*-dimensional vector $\mathbf{S} = (s_1, s_2, ..., s_M)$, where $s_i = \pm 1$ or 0 denotes the charge number [viz., valence]. In other words, the single-chain configuration of a weak polyelectrolyte system is specified by the multidimensional vector $\mathbf{X} = (\mathbf{R}, \mathbf{S})$. Similarly, the position and ionization state of ionizable segment *i* can be designated as $\mathbf{x}_i = (\mathbf{r}_i, s_i)$. A unique feature of weak polyelectrolyte systems is that the polymer charge is a dynamic variable coupled with the solution conditions and chain configurations. The dynamic coupling is responsible for the correlated behavior of polymer ionization due to ion-specific solvent-mediated interactions, local excluded volume effects, inter- and intrachain correlations, and long-range electrostatic interactions.

### *2.2 Ising density functional theory*

The main ideas of iDFT have been reported in our earlier work.[23] Briefly, the starting point is formulation of a grand-potential functional in terms of the single-chain distribution $\rho(\mathbf{X})$ and

the density profile $\rho_v(\mathbf{r})$ of monomeric species *v*. The theoretical development is focused on the intrinsic Helmholtz energy *F*, which is comprised of an ideal component, $F^{id}$, and an excess component $F^{ex}$. While $F^{id}$ is exactly known, $F^{ex}$ is derived with perturbation methods that account for both inter- and intramolecular correlations. We can determine the structure and thermodynamic properties of a weak polyelectrolyte system by solving a set of the Euler-Lagrange equations for the single-chain distribution and ionic density profiles

$$\rho(\mathbf{X}) = \exp\left\{-\beta[V_0^B(\mathbf{X}) + \mu^H(\mathbf{S}) + V^{ext}(\mathbf{X}) + \mu^{ex}(\mathbf{X}) - \mu]\right\}, \tag{2}$$

$$\rho_v(\mathbf{r}) = \exp\left\{-\beta[V_v^{ext}(\mathbf{r}) + \mu_v^{ex}(\mathbf{r}) - \mu_v]\right\} \tag{3}$$

where $V_0^B(\mathbf{X}) = V^B(\mathbf{X}) + V^{NB}(\mathbf{X})$ stands for the intramolecular potential energy of a single chain, which includes contributions from the bond potential $V^B(\mathbf{X})$ and non-bonded hard-sphere and electrostatic interactions $V^{NB}(\mathbf{X})$. In Eqs.(2-3), $V^{ext}(\mathbf{X})$ and $V_v^{ext}(\mathbf{r})$ are the external potential of the polymer chain in single-chain configuration $\mathbf{X}$ and that of monomeric species $v$ at position **r**, respectively; $\mu^{ex}(\mathbf{X}) = \delta F^{ex} / \delta\rho(\mathbf{X})$ and $\mu_v^{ex}(\mathbf{r}) = \delta F^{ex} / \delta\rho_v(\mathbf{r})$ represent the local excess chemical potentials of polymers and monomeric species, and $\mu^H(\mathbf{S})$ accounts for the change in the chemical potential due to the deprotonation/protonation of the ionizable segments of the weak polyelectrolytes.

For the tangent chain model considered in this work, the bond potential can be written in terms of the one-dimensional Dirac-delta function $\delta(r)$

$$\exp\left[-\beta V^B(\mathbf{X})\right] \sim \prod_{i=1}^{M-1} \delta\left[|\mathbf{r}_{i+1} - \mathbf{r}_i| - \sigma(s_i, s_{i+1})\right] \tag{4}$$

where $\sigma(s_i,s_{i+1})=[\sigma(s_i)+\sigma(s_j)]/2$, and the proportionality constant can be determined by the normalization the segment distributions. Eq.(4) ensures that neighboring segments are in contact with one another. In general, the hard-sphere diameter of a polymer segment depends on its valence owing to the solvation effect. On the other hand, the non-bonded component, $V^{NB}(\mathbf{X})$, is given by the pair potential for charged hard spheres [see Eq.(1)] between all monomers

$$V^{NB}\left(\mathbf{X}\right)=\sum_{i=1}^{M-1}\sum_{j>i}u_{i,j}\left[|\,\mathbf{r}_i-\mathbf{r}_j\,|;Z\left(s_i\right),Z\left(s_j\right)\right]. \tag{5}$$

This term ensures that the polymer chain is self-avoiding (i.e., hard spheres cannot overlap) and accounts for the direct coulomb interaction between charged segments at infinite dilution.

The chemical potential of a weak polyelectrolyte depends on the charge state of individual segments as described by the chemical equilibrium for deprotonation/protonation

$$\mu^H\left(\mathbf{S}\right)=\sum_{i=1}^{M}\Delta\mu_i^H\left(s_i\right)=-\sum_{i=1}^{M}s_ik_BT\left(\mathrm{pK}_i-\mathrm{pH}\right)\ln 10 \tag{6}$$

where $\Delta\mu_i^H\equiv -s_ik_BT\left(\mathrm{pK}_i-\mathrm{pH}\right)\ln 10$ is the change in grand potential of the system due to the ionization of a single polymer segment. In Eq.(6), $s_i=0$ means that the polymer segment is in its neutral state, $s_i=-1$ stands for the deprotonation of an acidic segment, and $s_i=+1$ for the protonation of a basic segment. The equilibrium constant of the deprotonation or protonation reaction, $\mathrm{K}_i$, depends on the identity of the ionizable site and temperature but not on the local solution composition.

In numerical implementation of the iDFT equations, we determine the density profiles of polymer segments from the propagator functions

$$\rho_i(\mathbf{r},s_i)=\exp\left\{-\beta\left[V_i^{ext}(\mathbf{r},s_i)+\mu_i^{ex}(\mathbf{r},s_i)+\Delta\mu_i^{H}(s_i)-\mu\right]\right\} \times\sum_{\{s'_{i-1}\}}G_i^{L}(\mathbf{r},s'_{i-1},s_i)\sum_{\{s'_{i+1}\}}G_i^{R}(\mathbf{r},s_i,s'_{i+1}) \tag{7}$$

where $V_i^{ext}$ and $\mu_i^{ex}$ are the external and excess chemical potential for the monomer *i* at position **r** in state $s_i$. $G_i^L$ and $G_i^R$ are propagator functions that account for the contribution of all other polymer segments given that segment *i* is at position **r** in charge state $s_i$. These propagator functions depend on the potential of mean force between polymer segments, the bond potential, and the one-body potential for all other segments besides *i*.

As the excess chemical potential of polymer segments and free ions are strongly coupled with their density profiles, Eq.(7), along with Eq.(3) for monomeric species, are normally solved with an iterative scheme. The numerical solution of these equations becomes computationally demanding when the intramolecular interactions are considered explicitly beyond neighboring segments because the propagator functions would then involve a multibody integration. In our previous work[23], we considered only intramolecular interactions between adjacent segments and thus, Eq.(2) could be conveniently solved in terms of segment density profiles that accounted for the charge status of either its left or right neighbor [viz., $\rho_i^{(2)}(\mathbf{r},s_i,s_{i+1})$ and $\rho_i^{(2)}(\mathbf{r},s_{i-1},s_i)$]. For polyelectrolytes, the neglect of interactions between non-neighboring segments is valid only at high salt conditions when the long-range electrostatic interactions are sufficiently screened.[28] An alternative method is thus necessary to comprehensively study weak polyelectrolyte systems where long-range intramolecular interactions are relevant. Direct simulation of such systems is computationally expensive due to the large number of degrees of freedom in a multi-chain system, although some recent efforts have shown progress in this direction[29-31]. The single-chain-in-mean-field (SCMF) algorithm allows us to generate an ensemble of polymer configurations in place of

the analytical evaluation of the propagator functions[24]. The so-generated single-chain distributions approximate the high-dimensional, single-chain distribution $\rho(\mathbf{X})$ in the external field, according to Eq. (2). The equilibrium distributions of polymer segments and ionic species are obtained through an iterative procedure as described in the following section.

### *2.3 Single-chain simulation of weak polyelectrolytes*

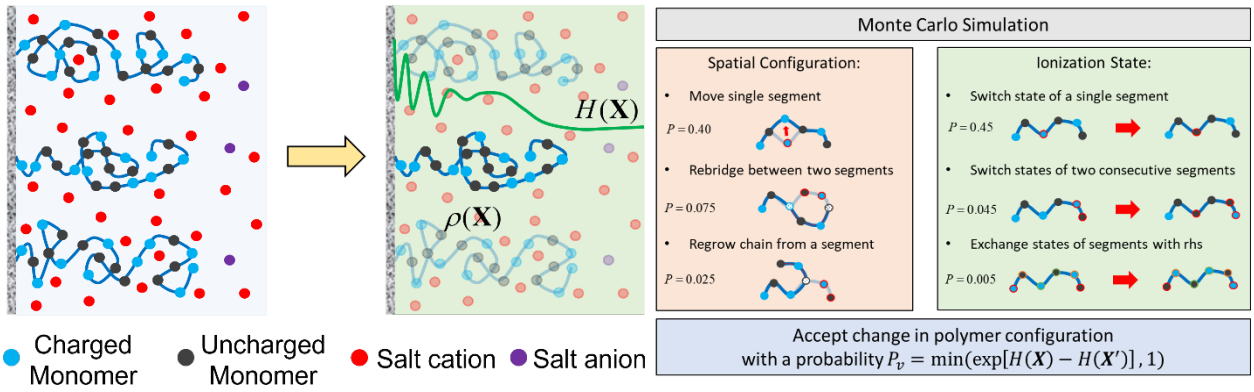


Figure 1. Schematic of the single-chain Monte-Carlo simulation in the presence of a one-body potential (viz., an effective external field) for each polymer segment. The simulated polymer may change its configuration and/or the ionization states of individual segments through various Monte-Carlo moves.

The single-chain-in-mean-field simulation represents a multichain system as a collection of single-chain ensembles subjected to an effective single-chain Hamiltonian $H(\mathbf{X})$. The effective single-chain Hamiltonian $H(\mathbf{X})$ accounts for the instantaneous intramolecular interactions explicitly while the complicated intermolecular interactions are replaced by an external field. The latter arises from the *averaged* intermolecular correlations of the polymer segments with other chemical species in the environment. In the context of the iDFT model discussed above, the single-chain Hamiltonian can be split into four components:

$$H(\mathbf{X}) = V_0^B(\mathbf{X}) + \mu^H(\mathbf{S}) + V^{ext}(\mathbf{X}) + \mu^{ex}(\mathbf{X}) \tag{8}$$

As discussed above, $V_0^B(\mathbf{X})$ stands for the intramolecular potential energy of a single chain, $\mu^H(\mathbf{S})$ represents the free energy of protonation or deprotonation of individual segments, $V^{ext}(\mathbf{X})$ is the external potential on the polymer, and $\mu^{ex}(\mathbf{X})$ is the local excess chemical potential for the polymer that accounts for the effects of inter- and intrachain correlations with all chemical species in the background. In other words, the last term accounts for the solution effects on the polymer configuration. The effective potential is decoupled from the single-chain ensemble and can be determined from iDFT instead of explicit simulation, which renders the name *mean-field* in single-chain-in-mean-field simulations. Note that the effective single-chain Hamiltonian, $H(\mathbf{X})$, depends on **X** because both the nonbonded potential and the thermodynamic effects depend on the positions of all chain segments as well as the charge states of polymer segments.

The single-chain Hamiltonian serves as an input into the single-chain Monte-Carlo simulation. In implementing the SCMF simulation, we first generate a set of *n* (~1000) *self-avoiding* polymer chains that do not explicitly interact with one another and instead interact implicitly through the effective field $H(\mathbf{X})$. A higher number of polymer chains has the benefit of a reduction in the fluctuations of the average properties but at the added expense of the computation time. For polymers grafted to a planar surface considered in this work, one of the end segments (designated as the first segment) is tangentially connected to a hard wall, which prohibits trespassing of any polymer segment. Each polymer chain satisfies the bonding constraint set by the freely jointed tangent chain model as given by Eq.(4), i.e., $|\mathbf{r}_{i+1} - \mathbf{r}_i| = \sigma$ where $\sigma$ is the hard-sphere diameter of the polymer segments. While iDFT is able to distinguish the identity of

individual segments in terms of both size and ionization behavior, we assume in this work that all polymer segments have the same hard-sphere diameter.

The single-chain Monte-Carlo simulation allows us to determine the density profile of polymer segment *i* from a set of single-chain configurations

$$\hat{\rho}_i(\mathbf{r}, s_i) = \frac{1}{\Delta_{bin}^3} \sum_{k=1}^{n} \theta\left( \frac{\Delta_{bin}}{2} - | x - x'_{k,i} | \right) \theta\left( \frac{\Delta_{bin}}{2} - | y - y'_{k,i} | \right) \theta\left( \frac{\Delta_{bin}}{2} - | z - z'_{k,i} | \right) \delta_{s_i s'_{k,i}} \qquad (9)$$

where $\Delta_{bin}$ is the width of the sampling bin (~$0.05\sigma$), $\theta(r)$ is the step function, i.e., it is unity when $r > 0$ and zero otherwise, and $\delta_{s_i s'_{k,i}}$ is the Kronecker delta function. During the single-chain Monte-Carlo simulation, we count segment *i* with charge state $s_i$ from all polymer chains that are simulated independently within the sampling cell $\mathbf{r} \pm \Delta_{bin}/2$. We divide the number in each bin by volume $\Delta_{bin}^3$ to determine the average density at position **r**.

The simulation protocol consists of trial displacements of polymer segments to update the configuration and the change in the charge state of each ionizable site. The latter is analogous to "spin flipping" in the Ising model except that here, the fluctuation of microstates is represented by changing the valence from 0 to +1/-1 or vice versa. The instantaneous densities of the polymer segments are calculated after each cycle of Monte-Carlo (MC) moves that on average allows for a complete update of the segment position and ionization state for all polymer segments. Figure 1 schematically shows the different simulation moves employed in this work. They consist of either the movement of a single polymer segment, the rebuilding of the polymer chain between two randomly selected segments *i* and *j*, or regrowing all segments that come after a randomly selected segment *i* (i.e., the chain segments $j > i$ are removed then these segments are placed back starting from segment *i*+1). The last two MC moves are instrumental in efficiently sampling the

configurational space of the polymer chain because the removed segments can adopt any new arrangement while maintaining tangent connection between adjacent monomers. The chain regrowing is less complicated as the replacement of segment $i$+1 only involves the constraint of tangent connection to segment $i$. However, for rebuilding the chain between segments $i$ and $j$, the placement of segment $i$+1 must be tangent to segment $i$ *and* allow for tangent connection between segments $j$-1 and $j$. Consequently, the configurational space is more restricted for the newly placed segments. In addition to configuration changes, we update the ionization states of each segment by randomly switching between charged and neutral states. The MC move is applied to a single segment, two consecutive segments, or the entire chain by exchanging the charge states of segments from 1 to $M/2$ with those for segments from $M$ to $M/2+1$ (which conserves the net charge of the polymer and its charge sequence order). In general, charge neutrality in the system is not maintained during a MC cycle as we consider the polymer charge to be a dynamic variable. However, charge neutrality is enforced after each cycle through the calculation of the density profiles of mobile ions from Eq.(3) which serves as a neutralizing background to the polymer charge. Therefore, our simulations are performed at a quasi-neutral state condition.

The single-chain MC moves are implemented to fulfill detailed balance. For instance, simple, single-segment MC moves are accepted with the standard Metropolis acceptance probability

$$P_{acc} = \min\left\{\exp\left[\beta H\left(\mathbf{X}_{old}\right) - \beta H\left(\mathbf{X}_{new}\right)\right], 1\right\} \tag{10}$$

where $\mathbf{X}_{new}$ and $\mathbf{X}_{old}$ refer to the new and old configurations of the polymer, respectively. Unfortunately, direct implementation of the MC moves in this manner can have a low acceptance rate because certain configurations are highly unfavorable or impossible (e.g., segment-segment

overlap in a hard-sphere chain). Because these low probability configurations would be rejected, a longer simulation would be required to properly sample the polymer configurations. To address this issue, we use the configurational bias Monte Carlo (CBMC) scheme to increase the likelihood of generating a new configuration that is accepted. For example, when rebridging a polymer, the next segment can be placed in different positions at random. The position of this next segment is then chosen based on the Boltzmann probability of the different trial positions. By CBMC sampling, we are able to increase the likelihood that the generated configuration would be accepted and thus avoid inefficient configuration sampling. From the generated configurations of the polymer chains determined from the MC cycle, we can determine the densities of the polymer segments by averaging over the *n* independent, single-chain configurations. The new polymer density profile will influence the local excess chemical potential of the polymer segments and ions, $\mu_i^{ex}(\mathbf{r}, s_i)$ and $\mu_v^{ex}(\mathbf{r})$, respectively.

The SCMF simulation results in the output of the density profile of the polymer segments $\rho_i(\mathbf{r}, s_i)$ for the polymers in the effective field $H(\mathbf{X})$. However, due to the interdependence of $H(\mathbf{X})$ and $\rho_i(\mathbf{r}, s)$, we must redetermine $H(\mathbf{X})$ every time $\rho_i(\mathbf{r}, s)$ is updated. To determine the effective field, we must first solve for the new distribution of all other species not included in the SCMF simulation (viz., the ions) due to their interactions with the polymer segments. From the perspective of the iDFT calculation, our system is described by a grand potential that incorporates the density profile of the polymer segments as a fixed quantity [see Eq.(S1)]. The new density distribution of ions $\rho_v(\mathbf{r})$ is determined by minimizing this grand potential using the Picard iteration. Typically, converging results for the ionic density profiles that satisfy Eq.(3) can be obtained within 200 iterations. With the appropriate solution to the grand potential, we can then determine the effective field $H(\mathbf{X})$ from Eq.(8). The cycle is repeated by performing a SCMF

simulation with the new $H(\mathbf{X})$ and so forth. Through these cycles, the system relaxes towards its equilibrium state and the properties of interest, such as the degree of ionization, fluctuate around their equilibrium values. We can then update the field (viz., one-body potentials) and perform single-chain simulation by tracking the properties of interest. The procedure terminates once the average values are converged.

**3. Results and discussion**

The numerical performance of sc-iDFT has been tested with a polyacid brush of length $M = 25$ at two grafting densities $\rho_{graft}$ = 0.10 and 1.00 #/nm$^2$. A similar system was considered in our earlier work with one-dimension (1D) iDFT calculations. The parameters were chosen to best represent experimental results for a poly(acrylic acid) brush in aqueous NaCl solutions (with $\sigma = 5.0$Å and $\mathrm{pK} = 4.756$)[32]. At moderate to high grafting density, the system is considered to be homogeneous in the xy-plane (parallel to surface) and thus the ion distribution varies only in the z-direction (perpendicular to the surface). At low grafting density, the assumption of lateral homogeneity breaks down because the polymer molecules no longer overlap with one another. Note that the density profiles are laterally averaged whereas the polymer configuration is in three-dimensional space; therefore, the long-wavelength fluctuation effects are not considered in the present work. The chain is simulated in the effective field determined from 1D-iDFT as outlined in Section 2.4 until the equilibrium morphology is obtained based on the convergence of the average properties including density profiles, brush thickness, and degree of ionization.

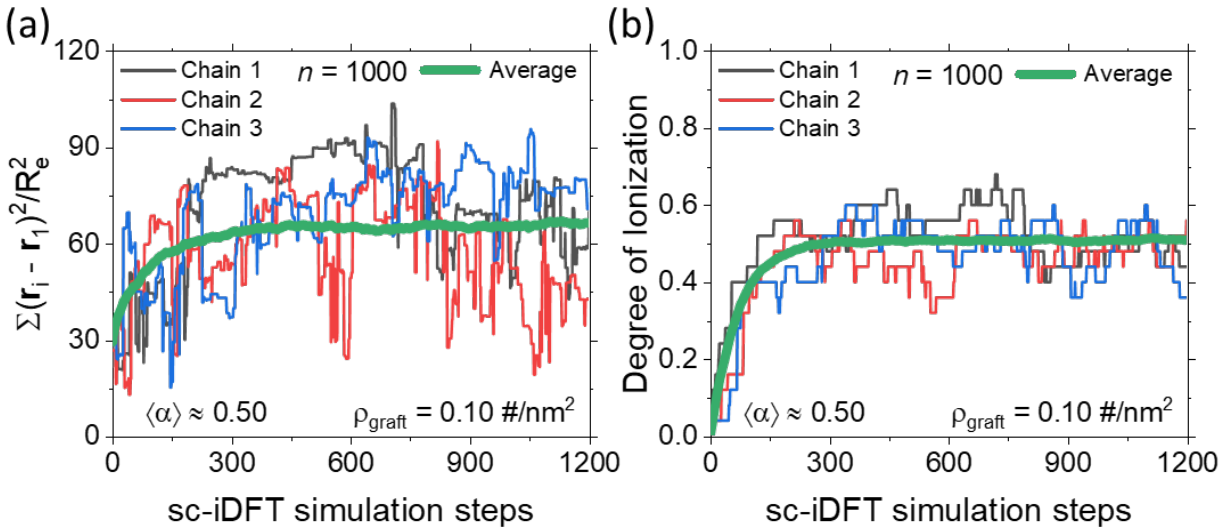


Figure 2. (a) The total distance between segment 1 and all other segments normalized by the square of the end-to-end distance and (b) the degree of ionization ($\alpha_p$) for three weak polyelectrolyte chains. The solid green line is the average for the given property over all chains ($n$ = 1000) at the same simulation step. Here, the salt concentration is 10 mM, the grafting density is 0.10 #/nm$^2$, and the chain length is 25, mimicking a poly(acrylic acid) brush in aqueous NaCl solutions (viz. $\sigma = 5.0\text{Å}$ and $\text{pK} = 4.756$).

Figure 2 illustrates the evolution of the configuration for three weak polyelectrolyte chains as a function of sc-iDFT simulation steps. Also shown in this figure are the degree of ionization and the average polymer configuration over all $n$ chains considered in parallel. Note that each polymer chain only interacts with the effective field $H(\mathbf{X})$ and therefore there is no explicit interaction between any chains. As expected, the single-chain configuration (viz., configuration and ionization state) fluctuates around the average configuration because of MC sampling. In general, we find that the relaxation time from the initial state to the equilibrium state is significantly longer for the conformation of the polymer than that for the ionization state. The faster relaxation of the ionization can be attributed to the fact that there are only two states (viz., charged and

uncharged) that tend to differ greatly in energy with many possible arrangements of these charged sites on the polymer chain. On the other hand, the configurational change relies on small movements of the polymer chain in a slowly varying external field. The regrowing move is particularly useful to accelerate the polymer relaxation time as it efficiently reconfigures the chain end (unlike bridging which can only influence internal configuration); thus, the configuration can quickly adapt to the updated field. It should be noted that the relaxation time is dependent on the arbitrary choice of how often a simulation move is executed. Therefore, fine-tuning the frequency of Ising Monte Carlo moves is crucial. This optimization ensures that the simulation does not invest excessive time in updating a quantity more frequently than required, thereby enhancing the efficiency of the overall process.

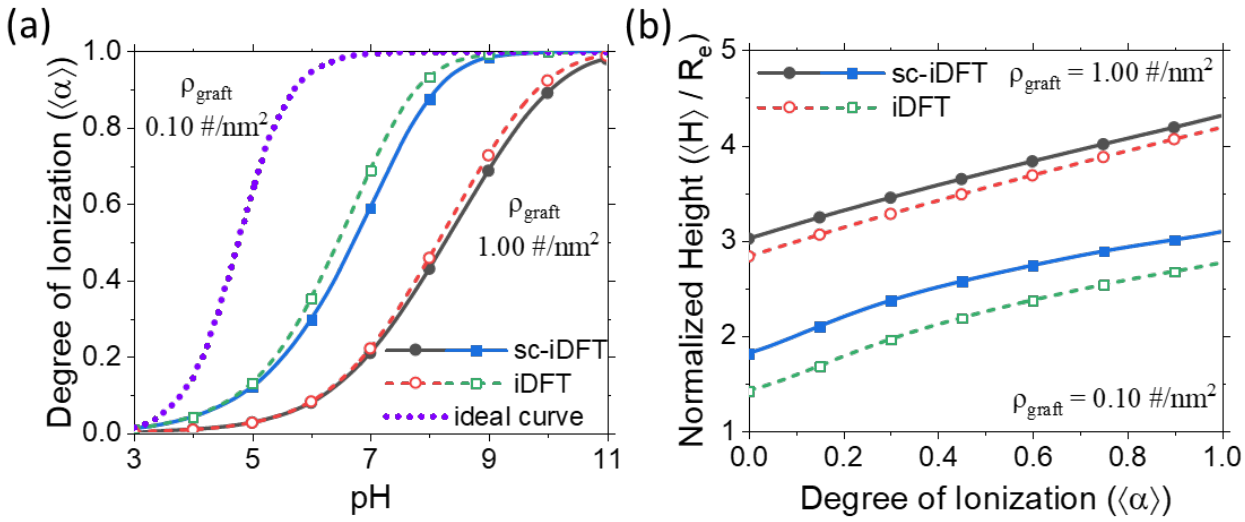


Figure 3. (a) Degree of ionization as a function of pH and (b) the normalized brush height as a function of degree of ionization for the model weak polyacid brush predicted by sc-iDFT (solid line) and iDFT (dashed line). The brush height is normalized by the end-to-end distance of an ideal chain ( $R_e = \sigma\sqrt{M-1}$ ). Here, the chain length is $M =$ 25, and the salt concentration is 10 mM. The two sets of lines correspond to two different grafting densities: 0.10 #/nm$^2$ and 1.00

#/nm$^2$ (or 0.025 #/$\sigma^2$ and 0.25 #/$\sigma^2$, respectively). In addition, the ideal titration curve is given by the dotted line.

Figure 3 compares the theoretical predictions of sc-iDFT and iDFT for the degree of ionization and the thickness of a weak polyacid brush. We see that the iDFT calculation predicts the earlier ionization of the polymer than predicted by sc-iDFT since the iDFT neglects the long-range intrachain interactions that are considered in sc-iDFT. The difference between the two methods is negligible when the grafting density is increased from 0.10 #/nm$^2$ to 1.00 #/nm$^2$. Since the intrachain correlations between the charged monomers are heavily influenced by the concentrations of the local charged species, the increase in grafting density of the polymer brush (and therefore the local charge density) drives more counterions to adsorb in this region and these counterions screen the intrachain electrostatic correlation (see Figure S3c). Thus, the long-range interactions are almost entirely screened at $\rho_{graft}$ = 1.00 #/nm$^2$, which leads to the similarity in the ionization results from iDFT and sc-iDFT. By comparison of either method to the ideal titration curve, we see that the intermolecular interactions play a significant role in dictating the polymer ionization. The non-ideal effects are also evident from the large shift of the titration curves at different grafting densities.

We expect that the deviation between iDFT and sc-iDFT will be greater as the brush grafting density is decreased below 0.10 #/nm$^2$, especially when the salt concentration is also decreased since the long-range correlations will become more significant. However, the calculation (whether iDFT or sc-iDFT) assumes the ion and polymer distribution to be homogeneous in the lateral directions, which may not be valid when the brush is sufficiently dilute. At dilute conditions, there will be a heightened presence of counterions near the polymer chains and a lower presence in between the polyelectrolytes. Interestingly, at dilute grafting densities, the

density distribution of ions is approximately the same as that in the bulk solution (see Figure S3a) because there is limited intermolecular interactions with the polymer and the surface is considered a hard wall (viz., it is uncharged). In this case, the intramolecular correlations dictate the polymer configuration since the intermolecular correlations are approximately uniform and equivalent to the bulk. We expect that sc-iDFT can accurately predict the properties of weak polymer brushes across a wide range of solution conditions because we account for both the inter- and intrachain correlations important for determining the polymer configuration and ionization.

Besides the degree of ionization, another point of comparison between the two methods is the thickness of the weak polyacid brush, shown in Figure 3b. As one expects from prior studies on weak polyelectrolyte brushes[13-15, 24, 33], the brush height increases when the grafting density is increased or the polymer gains more charge (i.e., an increase in the pH for a weak polyacid). The sc-iDFT and iDFT predictions differ even at low pH when the polymer is entirely uncharged (i.e., the long-range electrostatic interactions are not relevant) because sc-iDFT has the advantage of capturing the self-avoiding characteristic of a hard-sphere chain. In iDFT, segment-segment overlap between non-neighboring segments is allowed, whereas sc-iDFT restricts the polymer chain to only those configurations that satisfy self-avoidance through the nonbonded intrachain potential $V^{NB}(\mathbf{X})$. If we considered an ideal chain instead of a hard-sphere chain (i.e., allowed segment-segment overlap), the brush thickness from sc-iDFT would be equivalent to iDFT for the uncharged polymer. Interestingly, the ratio of brush thickness from sc-iDFT to iDFT decreases as the polymer gains more charge. When the brush is collapsed, the intrachain excluded volume plays a dominant role in dictating the configuration of the polymer. However, when the polymer is charged, the configuration is naturally extended due to the long-range Coulomb repulsion. Thus, the contribution of intrachain excluded volume effect is less relevant to the configuration of the

polymer because at such conditions, the Coulomb interaction will disfavor the overlap of the polymer segments. The difference in brush thickness predicted by the two methods is less noticeable at higher grafting densities since intermolecular correlations (viz. hard-sphere correlations and mean electrostatic potential) dominate the polymer configuration. By neglecting the long-range intramolecular interactions between the charged monomers in the polymer chain, iDFT and other polymer mean-field theories like the molecular theory[34] overestimate the polymer ionization while also underestimating the expansion of the weak polyelectrolyte brush. sc-iDFT marks a substantial improvement over existing methods by taking advantage of the single-chain Monte-Carlo simulation and coupling with the iDFT to treat the multibody state and configuration on equal footing.

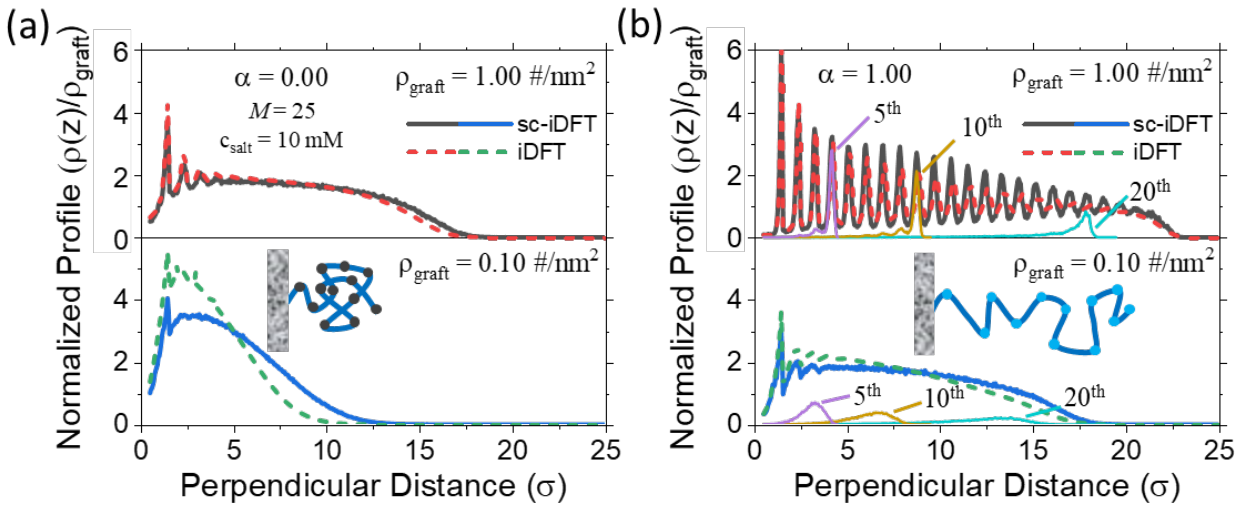


Figure 4. The normalized density profile, defined as $\rho(z)\sigma / \rho_{graft}$, for a polyacid brush when the polymer is (a) fully uncharged and (b) fully charged. The predictions by sc-iDFT and iDFT are given by the solid and dashed lines, respectively, at two different grafting densities: 0.10 #/nm$^2$ and 1.00 #/nm$^2$. The chain length is $M = 25$ and the salt concentration is 10 mM. Panel (b) also includes the density profile for segment numbers 5, 10, and 20 as predicted by sc-iDFT.

Figure 4 shows the density profiles of the weak polyacid brush at a grafting density of 0.10 #/nm$^2$ and 1.00 #/nm$^2$ when the brush is either neutral or fully charged. In the neutral brush case, the long-range electrostatic intrachain interactions are not present and therefore the difference between iDFT and sc-iDFT is solely due to the intrachain excluded volume that prevents segment-segment overlap in sc-iDFT. The statistics of a self-avoiding chain due to hard-sphere repulsion cannot be captured by iDFT since it requires explicit knowledge of the complete single-chain distribution. For this reason, the iDFT calculation, like other mean-field theories[34], becomes inaccurate at low grafting densities due to the inability to account for intrachain excluded volume. At high grafting density, the hard-sphere packing results in a strong oscillation in the density of segments perpendicular to the surface as seen previously in iDFT calculations[35]. This behavior is not well captured by alternative theories because they utilize an incompressibility condition[34]. In general, sc-iDFT predicts the polymer segments are distributed further away from the surface than that predicted by iDFT since the intrachain excluded-volume and electrostatic interactions will result in stretched configurations being favored. At high grafting density, both methods exhibit almost discrete peaks for the segment profile, which indicates that the brush is significantly stretched (i.e., rod-like). Further evidence for the stretched configuration of the brush can be seen by the density profiles for segment numbers 5, 10, and 20 in Figure 3b. These density profiles show a narrow region, in which the specific segment is present. In contrast to the segment profile for a brush with high grafting density, the segment profile at the low grafting density is broadened since the segments are not localized in a specific layer. A benefit of sc-iDFT is that directly sampling the polymer configuration in the effective field allows us to capture the rod-like behavior; such behavior would be difficult to quantify using a method that generates the configurations beforehand like in the molecular theory[16]. In the case of sc-iDFT, the extended structure of the

polymer persists further than that predicted by the iDFT calculations because long-range intrachain interactions favor the more rod-like configuration.

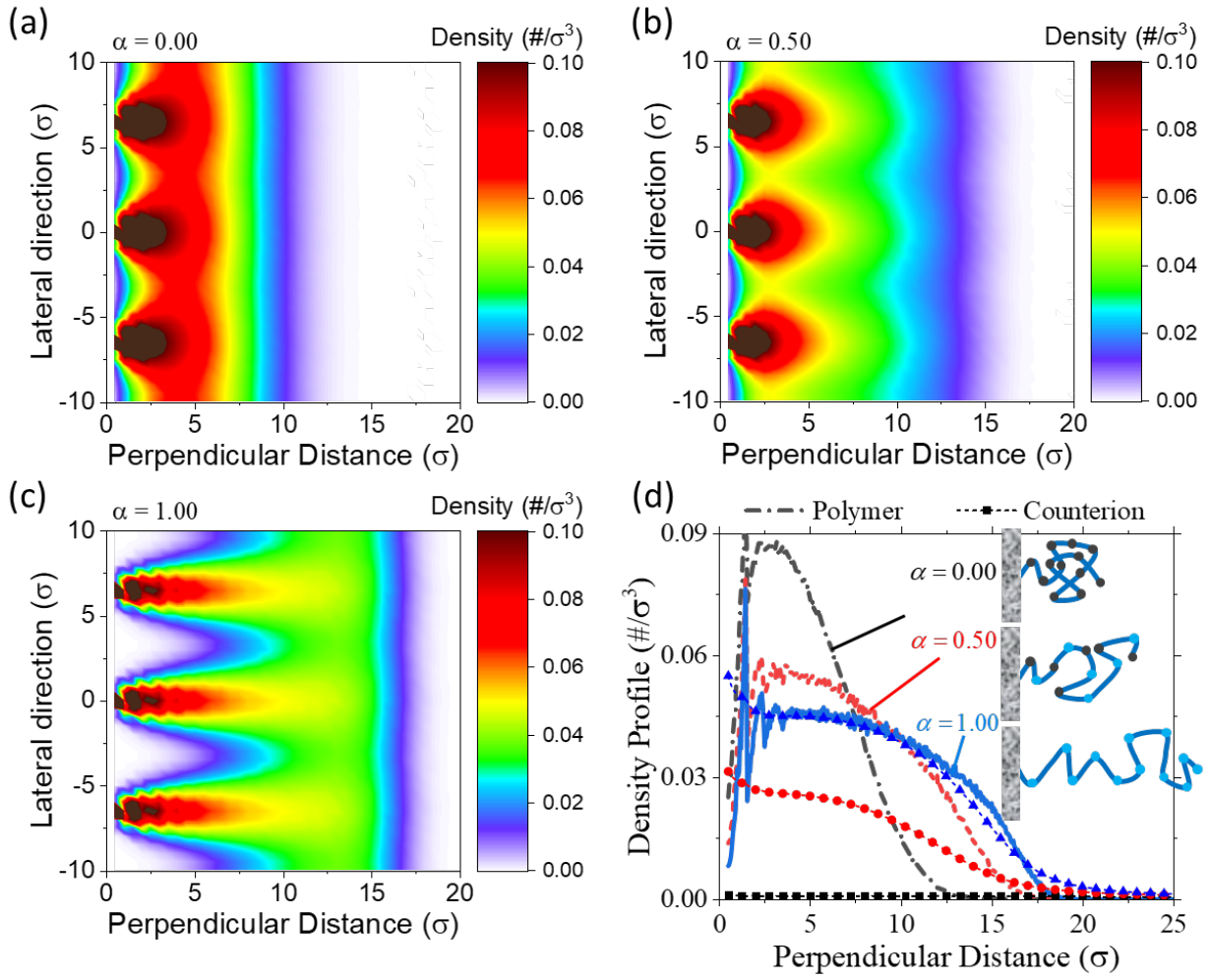


Figure 5. Two-dimensional view of the weak polyacid brush along the surface at three different degrees of ionization: (a) 0.00, (b) 0.50, and (c) 1.00. The chain length is $M = 25$ and the salt concentration is 10 mM. The grafting density of the brush is 0.10 #/nm$^2$. (d) The laterally averaged density profile of the polymer and its counterion (viz. cation salt) in the perpendicular direction from the surface at the three respective degrees of ionization.

In comparison to the one-dimensional implementation of iDFT, one major advantage of sc-iDFT is that it is able to account for the lateral correlations in the polymer configuration resulting from the intrachain correlations. In Figure 4, we show a two-dimensional view of the density profiles of polymer segments along the surface when the polyacid brush is uncharged, half-charged, and fully charged at an approximate grafting density of 0.10 #/nm$^2$ (viz. ~6.5 $\sigma$ units spacing between adjacent tethered points on a lattice surface). As mentioned previously, the lateral inhomogeneity in the distribution of ions should be accounted for when neighboring polymers do not overlap. We see that, at $\rho_{graft} = 0.10$ #/nm$^2$, there is still significant overlap between the grafted chains when the chain length is 25. Further decrease in the grafting density would result in an inhomogeneous distribution of the ions between the grafted points, which would affect the polymer configuration and ionization behavior of the brush. When the polymer is fully uncharged (Figure 5a), the brush is in a collapsed state and spreads across the surface. There is a significant overlap between neighboring polymers as evident by the increased density between the two grafting points. It should be noted that the polymer segments from one grafted chain are allowed to overlap with the polymer segments from a different grafted chain because the chains only interact through the single-chain Hamiltonian $H(\mathbf{X})$. Thus, intersegment overlap is not accounted for explicitly, but implicitly through the effective field. Previous implementations of polymer density functional theory have demonstrated that the intermolecular interactions can be reasonably well captured by an appropriate free energy functional[36].

Figure 5b shows the configuration behavior of the polymer when the brush is half-charged. In this case, the addition of Coulomb interactions in the brush lead to an expected extension of the brush perpendicular to the surface than what is seen in the uncharged case. The presence of charged segments within the brush results in electrostatic repulsions within the same polymer and

with segments of other tethered chains. Besides, the high density of localized polymer charges leads to the adsorption of counterions into the brush, leading to the brush swells due to the increased osmotic pressure. For a neutral brush, the polymer density decays from a large value as it extends farther from the surface since the repulsive forces are not strong enough to stretch the polymer chains. On the other hand, when the polymer is fully ionized as shown in Figure 5c, the brush is stretched to about 75% of its contour length. In this case, the interactions between the charged segments within a polymer chain, as well as with segments from other polymer chains, influence the extended configuration of the polymer. Due to the strong repulsion from other grafted chains, the tethered polymer is mostly extended perpendicular to the surface with very low density of segments between neighboring chains, particularly within the first 5 units from the surface.

Lastly, Figure 5d shows the laterally averaged density profiles of the polymer segments and its counterion (viz. cation salt) in the perpendicular direction from the surface. As expected from prior analysis, the brush transitions from a coiled state to a stretched state as it goes from uncharged to fully charged. In the fully charged case, the oscillatory density profile in the inner region of the brush indicates that the first few segments of the brush are mostly perpendicular to the surface. This configuration follows from the lack of segment density between the two brushes as seen in Figure 5c. Such insights into the configurational behavior of the polymer cannot be well described through iDFT calculations (even if the density profiles are not laterally averaged) since the configuration is dictated not only by intermolecular interactions, but also the intrachain interactions as described by sc-iDFT. The counterion profile is larger for a higher degree of ionization as expected since the salt cations compensate for the negatively charged brush. When the polymer is uncharged, the concentration of salt counterions in the brush region is comparable

to the concentration in the bulk. However, when the polymer is half-charged, the counterion concentration is greatly elevated compared to its bulk concentration and the profile is qualitatively similar to the brush profile, except the counterions are increased at the surface and there is no oscillation in the profile. For a fully charged brush, the counterions match the polymer segments in concentration except near the edge of the brush, in which the counterion profile decreases at a shorter distance from the surface but decays more slowly than the decay of the brush profile. The increased presence of counterions outside the brush region relative to the bulk concentration indicates that the entropic penalty of ion adsorption is not overcome by the driving force due to favorable electrostatic interactions between the counterion and charged polymer segments.

## 4. Conclusion

In summary, sc-iDFT provides a new theoretical procedure to account for the ionization-configuration coupling in weak polyelectrolyte systems that cannot be captured with conventional methods. It is numerically efficient compared to explicit particle-based Monte Carlo simulation by approximating the inter- and intramolecular interactions through an effective single-chain Hamiltonian determined via the Ising density functional theory (iDFT). A major advantage of sc-iDFT is that each chain is simulated independently of any other chain; therefore, it can be easily parallelized for GPU computing extending the application to more detailed, realistic polymeric systems. In addition, the inclusion of intrachain correlations beyond the nearest-neighbor level is important for understanding the charge-regulation and configuration behavior in hetero-weak polyelectrolytes such as zwitterionic polymers and polypeptides. While the discussion above has focused on a coarse-grained model, similar procedures can be established for other weak-polyelectrolyte models including those with atomistic details by incorporating the Ising degree of freedom to account for the charge states of ionizable sites.

It should be noted that sc-iDFT simulation allows us to determine not only the single-chain properties but also the thermodynamic of the entire multichain system. Averaged properties rapidly approach their equilibrium values with only minor fluctuations when a relatively small number (here $n = 1000$) of chains are considered. Since we sample the single-chain distribution $\rho(\mathbf{X})$, we obtain direct information about the configurational fluctuations. Our single-chain Monte-Carlo simulation, using rebridging and regrowing moves, efficiently samples the configurational space of tethered polyelectrolytes and rapidly relaxes the initial single-chain distribution to its equilibrium. In principle, sc-iDFT allows us to study the dynamics of the system by using only local moves (i.e., single bead movements). We will explore these ideas, along with the full 3-dimensional implementation of sc-iDFT in our future work.

**Acknowledgements**: This work is financially supported by the NSF-DFG Lead Agency Activity in Chemistry and Transport in Confined Spaces under Grant No. NSF 2234013 and Mu1674/18. Additional support is provided by the NSF Graduate Research Fellowship under Grant No. DGE-1326120.

**Data Availability:** The data that support the findings of this study are available from the corresponding author upon reasonable request.

**Supporting Information**: Equations for excess free energy in density functional theory and additional results for ionization and configuration behavior of weak polyelectrolytes.

**References:**

1. Yap, H. P.; Quinn, J. F.; Ng, S. M.; Cho, J.; Caruso, F., Colloid Surface Engineering via Deposition of Multilayered Thin Films from Polyelectrolyte Blend Solutions. *Langmuir* **2005,** *21* (10), 4328-4333.
2. Yuan, W.; Weng, G.-M.; Lipton, J.; Li, C. M.; Van Tassel, P. R.; Taylor, A. D., Weak polyelectrolyte-based multilayers via layer-by-layer assembly: Approaches, properties, and applications. *Advances in Colloid and Interface Science* **2020,** *282*, 102200.

3. Tong, W.; Gao, C.; Möhwald, H., Stable Weak Polyelectrolyte Microcapsules with pH-Responsive Permeability. *Macromolecules* **2006,** *39* (1), 335-340.
4. Ilyas, S.; Joseph, N.; Szymczyk, A.; Volodin, A.; Nijmeijer, K.; de Vos, W. M.; Vankelecom, I. F. J., Weak polyelectrolyte multilayers as tunable membranes for solvent resistant nanofiltration. *Journal of Membrane Science* **2016,** *514*, 322-331.
5. Muthukumar, M., 50th Anniversary Perspective: A Perspective on Polyelectrolyte Solutions. *Macromolecules* **2017,** *50* (24), 9528-9560.
6. Boroudjerdi, H.; Kim, Y.-W.; Naji, A.; Netz, R. R.; Schlagberger, X.; Serr, A., Statics and dynamics of strongly charged soft matter. *Physics reports* **2005,** *416* (3-4), 129-199.
7. Gonzalez Solveyra, E.; Nap, R. J.; Huang, K.; Szleifer, I., Theoretical modeling of chemical equilibrium in weak polyelectrolyte layers on curved nanosystems. *Polymers* **2020,** *12* (10), 2282.
8. Landsgesell, J.; Nová, L.; Rud, O.; Uhlík, F.; Sean, D.; Hebbeker, P.; Holm, C.; Košovan, P., Simulations of ionization equilibria in weak polyelectrolyte solutions and gels. *Soft Matter* **2019,** *15* (6), 1155-1185.
9. Biesheuvel, P. M.; van der Veen, M.; Norde, W., A Modified Poisson−Boltzmann Model Including Charge Regulation for the Adsorption of Ionizable Polyelectrolytes to Charged Interfaces, Applied to Lysozyme Adsorption on Silica. *The Journal of Physical Chemistry B* **2005,** *109* (9), 4172-4180.
10. Zhulina, E. B.; Borisov, O. V., Poisson–Boltzmann Theory of pH-Sensitive (Annealing) Polyelectrolyte Brush. *Langmuir* **2011,** *27* (17), 10615-10633.
11. Zhulina, E. B.; Birshtein, T. M.; Borisov, O. V., Theory of Ionizable Polymer Brushes. *Macromolecules* **1995,** *28* (5), 1491-1499.
12. Israels, R.; Leermakers, F. A. M.; Fleer, G. J.; Zhulina, E. B., Charged Polymeric Brushes: Structure and Scaling Relations. *Macromolecules* **1994,** *27* (12), 3249-3261.
13. Lyatskaya, Y. V.; Leermakers, F.; Fleer, G.; Zhulina, E.; Birshtein, T., Analytical self-consistent-field model of weak polyacid brushes. *Macromolecules* **1995,** *28* (10), 3562-3569.
14. Willott, J. D.; Murdoch, T. J.; Leermakers, F. A. M.; de Vos, W. M., Behavior of Weak Polyelectrolyte Brushes in Mixed Salt Solutions. *Macromolecules* **2018,** *51* (3), 1198-1206.
15. Witte, K. N.; Kim, S.; Won, Y.-Y., Self-Consistent Field Theory Study of the Effect of Grafting Density on the Height of a Weak Polyelectrolyte Brush. *The Journal of Physical Chemistry B* **2009,** *113* (32), 11076-11084.
16. Gong, P.; Genzer, J.; Szleifer, I., Phase Behavior and Charge Regulation of Weak Polyelectrolyte Grafted Layers. *Physical Review Letters* **2007,** *98* (1), 018302.
17. Gong, P.; Wu, T.; Genzer, J.; Szleifer, I., Behavior of Surface-Anchored Poly(acrylic acid) Brushes with Grafting Density Gradients on Solid Substrates: 2. Theory. *Macromolecules* **2007,** *40* (24), 8765-8773.
18. Tagliazucchi, M.; Li, X.; Olvera de la Cruz, M.; Szleifer, I., Self-Organized Polyelectrolyte End-Grafted Layers Under Nanoconfinement. *ACS Nano* **2014,** *8* (10), 9998-10008.
19. Blanco, P. M.; Madurga, S.; Garcés, J. L.; Mas, F.; Dias, R. S., Influence of macromolecular crowding on the charge regulation of intrinsically disordered proteins. *Soft Matter* **2021,** *17* (3), 655-669.
20. Settanni, G.; Brill, W.; Haas, H.; Schmid, F., pH-Dependent Behavior of Ionizable Cationic Lipids in mRNA-Carrying Lipoplexes Investigated by Molecular Dynamics Simulations. *Macromolecular Rapid Communications* **2022,** *43* (12), 2100683.

21. Staňo, R.; Košovan, P.; Tagliabue, A.; Holm, C., Electrostatically Cross-Linked Reversible Gels—Effects of pH and Ionic Strength. *Macromolecules* **2021,** *54* (10), 4769-4781.
22. Lunkad, R.; Barroso da Silva, F. L.; Košovan, P., Both Charge-Regulation and Charge-Patch Distribution Can Drive Adsorption on the Wrong Side of the Isoelectric Point. *Journal of the American Chemical Society* **2022,** *144* (4), 1813-1825.
23. Gallegos, A.; Ong, G. M. C.; Wu, J., Ising density functional theory for weak polyelectrolytes with strong coupling of ionization and intrachain correlations. *The Journal of Chemical Physics* **2021,** *155* (24), 241102.
24. Léonforte, F.; Welling, U.; Müller, M., Single-chain-in-mean-field simulations of weak polyelectrolyte brushes. *The Journal of Chemical Physics* **2016,** *145* (22), 224902.
25. Daoulas, K. C.; Müller, M., Single chain in mean field simulations: Quasi-instantaneous field approximation and quantitative comparison with Monte Carlo simulations. *The Journal of Chemical Physics* **2006,** *125* (18), 184904.
26. Müller, M., Dynamics of Nonequilibrium Single-Chain Configurations in Triblock Copolymers. *Macromolecules* **2021,** *54* (13), 6296-6311.
27. Gallegos, A.; Wu, J., Charge Regulation of Natural Amino Acids in Aqueous Solutions. *Journal of Chemical & Engineering Data* **2020,** *65* (12), 5630-5642.
28. Gallegos, A.; Wu, J. Z., Hierarchical Model of Weak Polyelectrolytes with Ionization and Configuration Consistency. *Macromolecules* **2023**.
29. Curk, T.; Yuan, J.; Luijten, E., Accelerated simulation method for charge regulation effects. *The Journal of Chemical Physics* **2022,** *156* (4).
30. Yuan, X.; Hatch, H. W.; Conrad, J. C.; Marciel, A. B.; Palmer, J. C., pH response of sequence-controlled polyampholyte brushes. *Soft Matter* **2023,** *19* (23), 4333-4344.
31. Landsgesell, J.; Hebbeker, P.; Rud, O.; Lunkad, R.; Košovan, P.; Holm, C., Grand-reaction method for simulations of ionization equilibria coupled to ion partitioning. *Macromolecules* **2020,** *53* (8), 3007-3020.
32. Gallegos, A.; Ong, G. M. C.; Wu, J., Thermodynamic non-ideality in charge regulation of weak polyelectrolytes. *Soft Matter* **2021,** *17* (40), 9221-9234.
33. Willott, J. D.; Murdoch, T. J.; Humphreys, B. A.; Edmondson, S.; Webber, G. B.; Wanless, E. J., Critical Salt Effects in the Swelling Behavior of a Weak Polybasic Brush. *Langmuir* **2014,** *30* (7), 1827-1836.
34. Gong, P.; Wu, T.; Genzer, J.; Szleifer, I., Behavior of surface-anchored poly (acrylic acid) brushes with grafting density gradients on solid substrates: 2. Theory. *Macromolecules* **2007,** *40* (24), 8765-8773.
35. Jiang, T.; Li, Z.; Wu, J., Structure and Swelling of Grafted Polyelectrolytes: Predictions from a Nonlocal Density Functional Theory. *Macromolecules* **2007,** *40* (2), 334-343.
36. Qing, L.; Jiang, J., Interfacial microstructure of neutral and charged polymer brushes: A density functional theory study. *The Journal of Chemical Physics* **2022,** *157* (22), 224904.